

Parallel entangling gate operations and two-way quantum communication in spin chains

Rozhin Yousefjani^{1,*} and Abolfazl Bayat^{1,†}

¹*Institute of Fundamental and Frontier Sciences, University of Electronic Science and Technology of China, Chengdu 610051, China*

The power of a quantum circuit is determined through the number of two-qubit entangling gates that can be performed within the coherence time of the system. In the absence of parallel quantum gate operations, this would make the quantum simulators limited to shallow circuits. Here, we propose a protocol to parallelize the implementation of two-qubit entangling gates between multiple users which are spatially separated and use a commonly sheared spin chain data-bus. Our protocol works through inducing effective interaction between each pair of qubits without disturbing the others, therefore, it increases the rate of gate operations without creating crosstalk. This is achieved by tuning the Hamiltonian parameters appropriately, described in the form of two different strategies. The tuning of the parameters, makes different bilocalized eigenstates responsible for the realization of the entangling gates between different pairs of distant qubits. Remarkably, the performance of our protocol is robust against increasing the length of the data-bus and the number of users. Moreover, we show that this protocol can accomplish two-way communication and stand out the decoherence effects.

I. INTRODUCTION

In order to achieve universal computation on a digital quantum simulator one requires the capability of performing arbitrary local single-qubit unitary rotations on every qubit as well as one type of two-qubit entangling gate between any pair of qubits [1]. The single-qubit unitary operations are performed locally through external control fields and have been implemented with very high fidelity in various physical setups. The two-qubit entangling gate, however, can only be realized through interaction between the two qubits [2] and have been realized in quantum dots [3, 4], dopant-based systems [5], optical lattices [6, 7], ion traps [8–12], superconducting devices [13, 14], Rydberg atoms [15] and diamond nitrogen-vacancy centers [16]. The demand for direct interaction makes the realization of two-qubit gates very challenging for distant qubits. Thus, several proposals have been put forward to mediate the interaction between distant qubits using a shuttled particle [17–19], a traveling wave packet [20–23], a shared spatially extended mode [24, 25] or a spin chain data-bus [26–29]. The latter, namely spin chain setups [30–34], are particularly useful for mediating the interaction between two distant qubits as they are made from the same physical systems as the logical qubits and hence eliminate the adversity of interfacing between different physical systems. The dynamics of spin chain systems have already been harnessed to implement different quantum gates between spatially separated qubits [29, 35–39].

One of the main challenges in current quantum simulators is the finite coherence time which restricts the total number of gates that can operate. In addition, many implementations of the two-qubit gates allow for only one or very few gates at each instance. This substantially reduces the operation rate of quantum processors and restricts their ability to realize deep circuits. To overcome this obstacle, in the context of state transfer, several ideas have been developed to mediate interactions between multiple qubits [40, 41] or exploit dense cod-

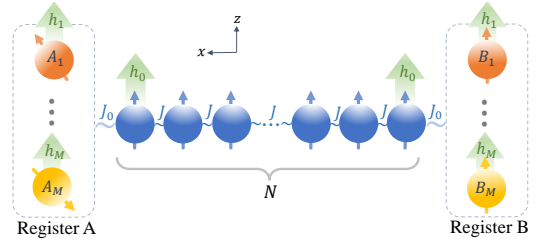


FIG. 1: The schematic of simultaneous entangling gates between M -pair qubits of registers A and B across a spin chain as data-bus. By appropriately modulating the exchange coupling J_0 , and local magnetic fields h_0 and h_ν ($\nu = 1, \dots, M$), each pair qubits $\{A_\nu, B_\nu\}$ would be mediated with a different set of system's energy levels.

ing like ideas in spin systems [28]. Current classical computers benefits from parallel computations by exploiting Multiple Instruction, Multiple Data (MIMD) architectures. This boosts their computational power while increasing the frequency scaling of their processors is practically impossible. Likewise, a quantum version of MIMD is highly desirable to design new protocols that are able to implement multiple entangling gates in parallel and enhance the operation rate within the coherence time of the hardware. Quantum gate parallelism which is essential for fault-tolerant error correction [42, 43] has so far been realized in ion-traps [44, 45] and optical lattices [6]. Nonetheless, the development of parallel operation of two-qubit gates between *selected* pair of qubits in the context of spin-based computation has remained a critical open question.

In this paper, we address this problem and put forward a protocol that implements parallel multiple two-qubit entangling gates on several distant pairs of qubits using a shared spin chain data-bus. The same setup can also be used for realizing two-way quantum communication which shows significant improvement over previous proposals [46]. The idea of this work is based on our previous work [47] which accelerates the rate of communication in quantum networks by allowing multiple users to simultaneously communicate through a common spin chain channel. To achieve parallel gate operation, we create an effective interaction between each pair

*Electronic address: RozhinYousefjani@uestc.edu.cn

†Electronic address: abolfazl.bayat@uestc.edu.cn

of users through properly tuning the Hamiltonian parameters. This is achieved through two different strategies which optimize different set of Hamiltonian parameters. Depending on the physical setup, one strategy might be more useful than the other. Finally, we investigate the robustness of the protocol in the presence of external noise which induces decoherence.

II. MODEL

We consider an array of N spin-1/2 particles as our data-bus in which particles interact via XX Hamiltonian

$$H_{ch} = J \sum_{i=1}^{N-1} (\sigma_i^x \sigma_{i+1}^x + \sigma_i^y \sigma_{i+1}^y) + h_0 (\sigma_1^z + \sigma_N^z), \quad (1)$$

where $\sigma_i^{x,y,z}$ are the Pauli operators acting on site i , J is the spin exchange coupling and h_0 represents the transverse magnetic field acting only on the end sites. We assume this spin-chain is shared between two remote quantum registers A and B, each containing M spin qubits labeled by A_ν and B_ν ($\nu = 1, \dots, M$), see Fig. 1. The interaction between the registers' qubits and the data-bus is given by

$$H_I = J_0 \sum_{\nu=1}^M (\sigma_{A_\nu}^x \sigma_1^x + \sigma_{A_\nu}^y \sigma_1^y + \sigma_N^x \sigma_{B_\nu}^x + \sigma_N^y \sigma_{B_\nu}^y) + \sum_{\nu=1}^M h_\nu (\sigma_{A_\nu}^z + \sigma_{B_\nu}^z), \quad (2)$$

where J_0 denotes the coupling between the registers and the data-bus and h_ν is the transverse magnetic field applying on the pair spin qubits $\{A_\nu, B_\nu\}$. We assume that qubits of the register A (B) are initially prepared in the normalized states $|\psi_\nu\rangle_A = \alpha_\nu^0 |0_\nu\rangle + \alpha_\nu^1 |1_\nu\rangle$ ($|\varphi_\nu\rangle_B = \beta_\nu^0 |0_\nu\rangle + \beta_\nu^1 |1_\nu\rangle$), and are decoupled from the data-bus which is initialized in the state $|\mathbf{0}\rangle_{ch} = |0, \dots, 0\rangle_{ch}$. Therefore, the state of the whole system becomes

$$|\Psi(0)\rangle = |\psi_1, \dots, \psi_M\rangle_A |\mathbf{0}\rangle_{ch} |\varphi_1, \dots, \varphi_M\rangle_B. \quad (3)$$

Once the coupling J_0 is switched on at time $t=0$, this quantum state evolves as $|\Psi(t)\rangle = e^{-iHt} |\Psi(0)\rangle$, where $H = H_{ch} + H_I$ is the total Hamiltonian of the system.

In Ref. [47], a protocol for simultaneous quantum communication between multiple users across a shared spin chain data-bus was proposed. In that protocol, one can achieve simultaneous high-fidelity state transfer between qubit pairs $\{A_\nu, B_\nu\}$, with low crosstalk, through appropriately tuning the local Hamiltonian parameters, namely J_0 , h_0 , and h_ν . Such tuning creates bilocalized eigenstates between each pair of users, namely qubits $\{A_\nu, B_\nu\}$, which then mediate direct interaction between them without affecting the others. According to Ref. [47], the tuning of the parameters for simultaneous state transfer requires the following steps:

- (I) Establishing an effective end-to-end interaction, i.e. confining the excitations to the qubits of the registers and leaving the channel approximately unexcited, i.e.

$|\mathbf{0}\rangle_{ch}$, at all times, by either decreasing J_0 [48–53] or increasing h_0 [40, 54] or both.

- (II) Making each pair of qubits $\{A_\nu, B_\nu\}$ off-resonant from the others through tuning the local magnetic fields h_ν .

Here, we extend these results to perform parallel multiple two-qubit entangling gates on pairs of qubits in the registers A and B. We also find out that the same protocol can be used for two-way communication.

In the case of $M=1$, the condition (I) and the free fermionic nature of the model results in dynamics which at a certain time $t = \tau$ can be well approximated as [28, 35]

$$e^{-iH\tau} |a_1\rangle_A |\mathbf{0}\rangle_{ch} |b_1\rangle_B \simeq e^{i\phi_{a_1 b_1}^1} |b_1\rangle_A |\mathbf{0}\rangle_{ch} |a_1\rangle_B. \quad (4)$$

Remarkably, for different choices of $a_1, b_1 = 0, 1$, at time $t = \tau$, the phases ϕ_{ab} take values such that [35]

$$\phi_{00}^1 = 0, \quad \phi_{01}^1 = \phi_{10}^1 = (N+1)\pi/2, \quad \phi_{11}^1 = N\pi, \quad (5)$$

where ϕ_{00}^1 is taken to be zero as the reference and $\phi_{10}^1 = \phi_{01}^1$ is guaranteed due to the mirror symmetry of the system. Therefore, this dynamics performs a quantum gate G_1 between the two qubits of the registers A and B

$$G_1 |a_1\rangle_A |b_1\rangle_B \simeq e^{i\phi_{a_1 b_1}^1} |b_1\rangle_A |a_1\rangle_B. \quad (6)$$

This gate not only swaps the qubits of the registers, but also imprints a phase which depends on the initial state of the qubits. The resulted phases at time $t = \tau$, given in Eq. (5), makes G_1 an entangling gate which creates a maximally entangled state between the two qubits if they start with $|\psi_\nu\rangle_A |\varphi_\nu\rangle_B = |+\rangle_A |+\rangle_B$, where $|+\rangle = (|0\rangle + |1\rangle)/\sqrt{2}$. The goal of this paper is to generalize these results to multiple users, namely $M > 1$, where the dynamics performs several two-qubit gates on the pairs $\{A_\nu, B_\nu\}$ (for $\nu = 1, \dots, M$) in parallel.

In the case of $M > 1$, the initial state of Eq. (3) takes the form

$$|\Psi(0)\rangle = \sum_{\mathbf{a}, \mathbf{b}} \alpha_{\mathbf{a}} \beta_{\mathbf{b}} |\mathbf{a}\rangle_A |\mathbf{0}\rangle_{ch} |\mathbf{b}\rangle_B, \quad (7)$$

where vectors $|\mathbf{a}\rangle_A = |a_1, \dots, a_M\rangle_A$ and $|\mathbf{b}\rangle_B = |b_1, \dots, b_M\rangle_B$ with $a_\nu, b_\nu = 0, 1$, denote the computational basis of the registers A and B, respectively, and $\alpha_{\mathbf{a}} = \prod_{\nu=1}^M \alpha_\nu^{a_\nu}$ and $\beta_{\mathbf{b}} = \prod_{\nu=1}^M \beta_\nu^{b_\nu}$ are abbreviations for multiplied coefficients of the initial states. Notably, satisfying the condition (I) leads to the emergence of bilocalized eigenstates whose excitations are mainly localized at the sites of the registers' qubits. These bilocalized eigenstates mediate the coupling between the computational states of the registers. By applying local magnetic field h_ν and meeting the condition (II), the excitations would be more localized between only two qubits, namely A_ν and B_ν (see Appendix C in Ref [47]). This can be achieved by properly optimizing h_ν 's to be adequately far from each other. Since the bilocalized eigenstates are the only ones involving in the dynamics of the system, each qubit pair $\{A_\nu, B_\nu\}$ evolves without disturbing the others and the channel mostly remains unexcited. In that

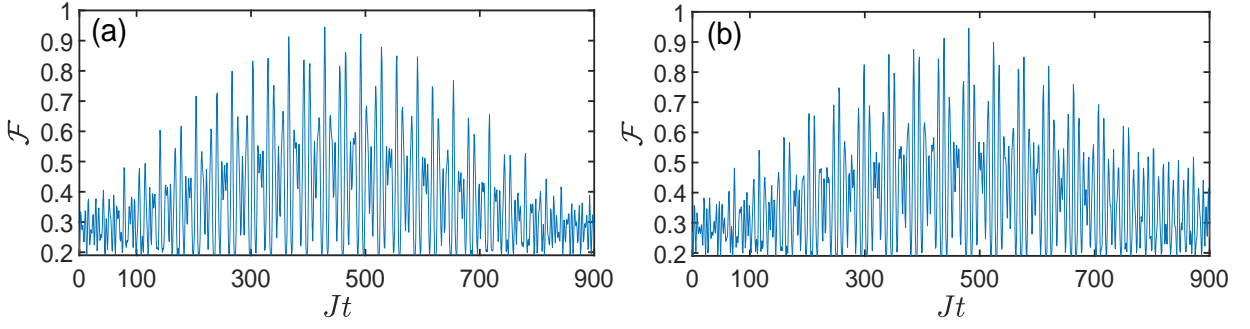


FIG. 2: $M=2$: The average $\mathcal{F}=(\bar{F}_1 + \bar{F}_2)/2$ for our two strategies **S1** (a) and **S2** (b) as a function of time in a chain of $N=20$. The Hamiltonian parameters for **S1** and **S2** are taken as $\{J_0^{opt}/J=0.04, h_1^{opt}/J=0.35, h_2^{opt}/J=-0.25\}$ and $\{h_0^{opt}/J=25, h_1^{opt}/J=0.4, h_2^{opt}/J=-0.25\}$, respectively.

case, the dynamics of the system at special time $t = \tau$ leads to

$$e^{-iH\tau}|a\rangle_A|0\rangle_{ch}|b\rangle_B \simeq e^{i\Phi_{ab}}|b\rangle_A|0\rangle_{ch}|a\rangle_B, \quad (8)$$

where $\Phi_{ab} = \sum_{v=1}^M \phi_{a_v, b_v}^v$ and again the mirror symmetry implies $\Phi_{ab} = \Phi_{ba}$. This state inversion allows us to introduce a global gate G between registers A and B as

$$G|a\rangle_A|b\rangle_B \simeq e^{i\Phi_{ab}}|b\rangle_A|a\rangle_B. \quad (9)$$

The special form of Φ_{ab} allows to write $G \simeq G_1 G_2 \dots G_M$, where G_v , is the two-qubit gate which acts on pair v , similar to Eq. (6).

The evolution in Eqs. (4) and (8) are very ideal and in reality, there are two main issues which deviate this perfect picture. The first one is the small dispersion in the system which leaks some information to the channel [55, 56]. The second issue is that the cross talk is not exactly zero and some information may leak to other pairs. These effects induce some entanglement between the data-bus and the registers, preventing the gate G and consequently G_v 's from being perfect unitary operations. In that case, the dynamics of each pair $\{A_v, B_v\}$ should be considered as a completely positive and trace preserving map, $\rho_v(t) = \Lambda^v(t)[\rho_v(0)]$. Here, $\Lambda^v(t)[\rho_v(0)] = T_{r_{\bar{v}}}(\Psi(t))\langle\Psi(t)|$ in which $T_{r_{\bar{v}}}$ means trace over all qubits except the pair $\{A_v, B_v\}$. To measure how well the map $\Lambda^v(t)$ approximates each two-qubit gate G_v , one can use the average gate fidelity [57]

$$\bar{F}_v(t) = \int d\psi \langle \psi | \psi \rangle G_v^\dagger \Lambda^v(t) [|\psi\rangle\langle\psi|] G_v |\psi\rangle, \quad (10)$$

where the integral is over the uniform (Haar) measure $d\psi$ on two-qubit state space, normalized as $\int d\psi = 1$. Rewriting Eq. (10) in the two-qubit computational basis, combined with some straightforward calculations, leads to

$$\bar{F}_v(t) = \frac{1}{5} + \frac{1}{20} \sum_{i'j'j} (G_v^*)_{ij} \langle i | \Lambda^v(t) [|j\rangle\langle j'|] |i'\rangle (G_v)_{j'j}. \quad (11)$$

Our goal is to maximize the average gate fidelity \bar{F}_v for all pairs $\{A_v, B_v\}$ at the same time. This can be pursued by maximizing the average $\mathcal{F} = \sum_{v=1}^M \bar{F}_v / M$ via controlling the Hamiltonian parameters J_0 , h_0 and h_v 's. Our protocol can be established in two different strategies based on the set of the

Hamiltonian parameters which are chosen to be optimized. In our first strategy, labeled by **S1**, we set $h_0=0$ and attempt to create effective end-to-end interaction via optimizing $J_0 < J$. In the second strategy, **S2**, this effective interaction would be induced by applying strong magnetic field $h_0 > J$ on the end sites of the data-bus while the coupling are kept uniform, i.e., $J_0=J$. Each of these strategies might be suitable for a different physical platform. Throughout the paper and for both strategies, we fix the time window to be $t \in [0, 500]/J$, for the dynamics of the system and then maximize the average gate fidelity \mathcal{F} with respect to the Hamiltonian parameters to find their optimal values, namely J_0^{opt}/J , B_0^{opt}/J and B_v^{opt}/J , as well as the gate duration τ at which the gate operation between each pair of qubits takes place. For the sake of clarity, the average gate fidelity \mathcal{F} that is obtained for the optimal parameters and the desired gate duration τ is denoted as $\mathcal{F}^{max} = \sum_{v=1}^M \bar{F}_v^{max}(\tau) / M$. In the following, we first restrict ourselves to the case of $M=2$, and evaluate the performance of two strategies **S1** and **S2**. Then, we extend the results to larger M .

A. Parallel gate operation for $M=2$

In this section we present the numerical results for the case of two parallel gate operations. For strategy **S1**, the average gate fidelity $\mathcal{F}=(\bar{F}_1 + \bar{F}_2)/2$ as a function of time in chain of length $N=20$ is plotted in Fig. 2(a). Here, the Hamiltonian parameters are optimized within the chosen time interval, namely $t \in [0, 500]/J$. The coupling J_0 is tuned to the optimized value $J_0^{opt}/J=0.04$, which results in an effective end-to-end interaction. Furthermore, we apply the optimized local magnetic fields $h_1^{opt}/J=0.35$ and $h_2^{opt}/J=-0.25$ on pairs $\{A_1, B_1\}$ and $\{A_2, B_2\}$, respectively, to make them energetically off-resonant and, hence, block the flow of information between them. For our second strategy **S2** the time evolution of $\mathcal{F}=(\bar{F}_1 + \bar{F}_2)/2$ is plotted in Fig. 2(b) for a chain of length $N=20$ and optimized Hamiltonian parameters as $h_0^{opt}/J=25$ for magnetic field applied to the end sites of the chain and $h_1^{opt}/J=0.4$ and $h_2^{opt}/J=-0.25$ for the magnetic fields applied on the pairs $\{A_1, B_1\}$ and $\{A_2, B_2\}$, respectively. As the figures show, the average gate fidelities for both strategies evolve in time and at a spatial time $t=\tau$ peak to their highest values which is more than 0.94. In other words, by letting the system

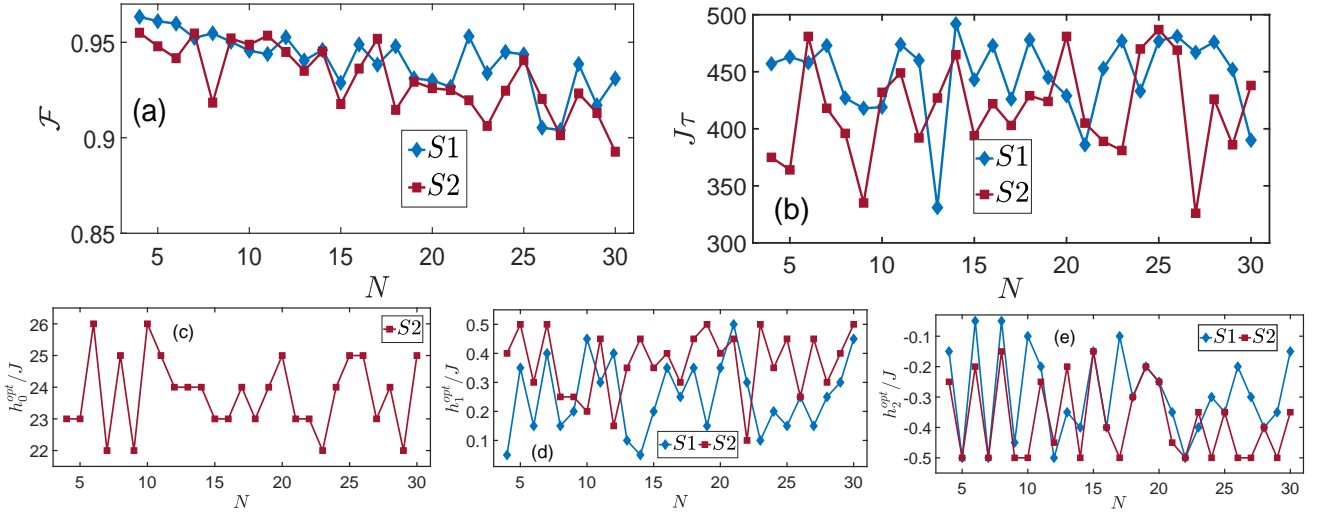


FIG. 3: $M = 2$: (a) The scaling of optimal average gate fidelity $\mathcal{F}^{max} = (\overline{F}_1^{max}(\tau) + \overline{F}_2^{max}(\tau))/2$ with N for strategies $S1$ and $S2$. (b) The desired gate duration $\tau \in [1, 500]/J$. (c) the optimal local magnetic field $h_0^{opt}/J \in [20, 40]$ for establishing effective end-to-end interaction in $S2$, (d) and (e) the optimal magnetic fields on registers' qubits $h_v^{opt}/J \in (-1)^{v+1}[0, 0.5]$ ($v = 1, 2$) for making the pair qubits off-resonant.

to evolve for $t = \tau$ one can perform two parallel entangling gate between the pairs $\{A_1, B_1\}$ and $\{A_2, B_2\}$, simultaneously.

We plot the scaling of $\mathcal{F}^{max} = (\overline{F}_1^{max}(\tau) + \overline{F}_2^{max}(\tau))/2$ with N in Fig. 3(a) for our both strategies. As the length increases the gate fidelity decreases slowly. Nonetheless, even for a pretty long chain of size $N = 30$ the gate fidelity \mathcal{F}^{max} still exceeds 0.92. This shows the high-quality performance of parallel gate operation between two pairs of users. As the results illustrate, in chain with large scale, the first strategy offers better performance over the second one in terms of the gate fidelity. The desired gate duration $\tau \in [1, 500]/J$ for different N 's is plotted in Fig. 3(b) for both $S1$ and $S2$ and its irregular fluctuations comes as a consequence of the fast oscillations in \mathcal{F} due to applied local magnetic fields h_v 's. In the case of $S1$, the optimal exchange coupling $J_0^{opt}/J \in [0.01, 1]$ behaves independent from the chain length and is obtained as 0.04 for all N 's, consisting with the results of [47, 48]. In our second strategy, the optimal magnetic fields on the end sites of the chain, i.e., $h_0^{opt}/J \in [20, 40]$, is reported in Fig. 3(c) and shows that for the considered chains, applying $21 < h_0^{opt}/J < 27$ is adequate for establishing effective end-to-end interaction between registers. The reminding Hamiltonian parameters, i.e., $h_v^{opt}/J \in (-1)^{v+1}[0, 0.5]$ ($v = 1, 2$), are plotted in Figs. 3(d) and (e) as functions of N . Here, the optimal magnetic fields on the pairs $\{A_1, B_1\}$ and $\{A_2, B_2\}$ are optimized over intervals with opposite sign to increase their energy detuning.

B. Parallel gate operation for $M > 2$

In this section we show that the parallel gate operation can be extended beyond $M = 2$. In fact, arbitrary number of parallel gates can be performed using our outlined strategies. In TABLE I, we present the performance of our protocol for the case of $M=3$ by adopting two strategies $S1$ and $S2$ for dif-

ferent chains. Here, $\mathcal{F}^{max} = (\overline{F}_1^{max}(\tau) + \overline{F}_2^{max}(\tau) + \overline{F}_3^{max}(\tau))/3$ is obtained after embedding the optimal values of the Hamiltonian parameters, i.e., $J_0^{opt}/J \in [0.01, 1]$, $h_0^{opt}/J \in [20, 40]$, and $h_v^{opt}/J \in (-1)^{v+1}[0, 1.5]$ ($v = 1, 2, 3$), presented in TABLE I. As results show, regardless of the adopted strategy, the gate fidelity achieves very high values such that \mathcal{F}^{max} remains larger than 0.91 even for chains up to $N=20$. Similar to the case of $M=2$, the first strategy presents better performance than the other one for long chains.

To highlight the advantages offered by our parallel gate operation protocol, in TABLE II we report \mathcal{F}^{max} and the optimal time τ for simultaneously implanting $M = 4$ entangling gates across a chain of length $N=4$. Surprisingly, for the both strategies, the average gate fidelities are steadily high and comparable with the case of single entangling gate, i.e., $M=1$. Moreover, a comparison between desired gate duration τ for different M shows that increasing the number of gates does not change the gate duration domain, which means that our protocol remarkably accelerates the rate of implementing two-qubit gates with no extra cost.

III. PERFORMANCE UNDER REALISTIC CONDITIONS

Decoherence effects, resulted by the fluctuating magnetic or electric fields in the environment, are unavoidable in practice. In this section we analyze the robustness of our protocol against such effects. We assume that the noise in the environment is Markovian which is described by a Lindblad master equation

$$\frac{d\rho(t)}{dt} = -i[H, \rho(t)] + \gamma \sum_i (\sigma_i^z \rho(t) \sigma_i^z - \rho(t)), \quad (12)$$

where γ represents the strength of decoherence. The first term on the right-hand side is unitary evolution imposed by the

N		5	10	15	20
$\mathcal{S}1$	\mathcal{F}^{max}	0.978	0.968	0.952	0.947
	$J\tau$	446	438	476	435
	J_0^{opt}/J	0.04	0.04	0.04	0.04
	h_1^{opt}/J	0.4	0.5	0.2	0.35
	h_2^{opt}/J	-0.3	-0.1	-1.2	-0.25
	h_3^{opt}/J	0.35	0.4	0.6	0.05

N		5	10	15	20
$\mathcal{S}2$	\mathcal{F}^{max}	0.977	0.963	0.947	0.919
	$J\tau$	459	472	482	500
	h_0^{opt}/J	26	25	26	28
	h_1^{opt}/J	0.5	0	0.2	1
	h_2^{opt}/J	-1.1	-0.7	-0.7	-0.6
	h_3^{opt}/J	1.1	1.2	1	1.2

TABLE I: $M=3$: The maximum of \mathcal{F} for gate duration $\tau \in [1, 500]/J$ by adopting strategies 1 and 2 in different chains. Here, the optimal exchange coupling J_0^{opt}/J for strategy $\mathcal{S}1$ has been optimized over the interval $J_0^{opt}/J \in [0.01, 1]$ and the optimal local magnetic field on the ends of the chain h_0^{opt}/J for $\mathcal{S}2$ has been optimized over $h_0^{opt}/J \in [1, 40]$. In both strategies, the optimal values for the local fields on qubits of the registers, i.e., h_1^{opt}/J , h_2^{opt}/J and h_3^{opt}/J , have been optimized over the interval $(-1)^{v+1}[0, 1.5]$.

M		1	2	3	4
$\mathcal{S}1$	\mathcal{F}^{max}	0.996	0.970	0.969	0.945
	$J\tau$	482	458	458	365
	J_0^{opt}/J	0.04	0.04	0.04	0.05
	h_1^{opt}/J	0.1	0.05	0.15	0.1
	h_2^{opt}/J	-	-0.15	-0.25	-1.4
	h_3^{opt}/J	-	-	0.05	1.2
	h_4^{opt}/J	-	-	-	-1

M		1	2	3	4
$\mathcal{S}2$	\mathcal{F}^{max}	0.991	0.967	0.956	0.925
	$J\tau$	489	376	474	391
	h_0^{opt}/J	26	23	24	25
	h_1^{opt}/J	0.25	0.4	0	0.4
	h_2^{opt}/J	-	-0.25	-1.4	-1.3
	h_3^{opt}/J	-	-	1.5	1.4
	h_4^{opt}/J	-	-	-	-0.3

TABLE II: Comparison: The maximum of \mathcal{F} and desired gate duration $\tau \in [1, 500]/J$ for different number of pairs $M = 1, \dots, 4$ in a chain with $N = 4$ by adopting outlined strategies. In the case of $\mathcal{S}1$, the optimal exchange coupling, J_0^{opt}/J , is obtained by surfing on the interval $[0.01, 1]$. The optimal magnetic field, h_0^{opt}/J , is optimized over $[20, 40]$ for the case of $\mathcal{S}2$. In both strategies and for all M 's the optimal local magnetic fields on the registers' qubits, h_v^{opt}/J ($v = 1, \dots, 4$), are optimized over $(-1)^{v+1}[0, 1.5]$.

Hamiltonian. The second part is the dephasing noise resulted by σ_i^z operators which act independently at each site. Without loss of generality, here, we restrict ourselves to the case of $M=2$ and consider the performance of our two strategies $\mathcal{S}1$ and $\mathcal{S}2$ in a spin-chain of $N=10$ as γ increases. The gate fidelity versus decoherence rate γ/J is plotted in Fig. 4. The Hamiltonian parameters for each strategy are taken in a way that if $\gamma=0$, then $\mathcal{F}=\mathcal{F}^{max}$. Obviously, there is no superiority between our two strategies in terms of the deterioration's rate and, as expected, the functionality of the gates is destroyed by increasing the dephasing rate. Nonetheless, for γ less than $10^{-4}J$ one can get $\mathcal{F}>0.9$.

IV. TWO-WAY QUANTUM COMMUNICATION

In Ref. [46], the authors propose a two-way quantum communication setup in which two users can exchange quantum states at the same type using the same spin chain data-bus, with very low fidelity. Our protocol for implementing parallel two-qubit gates can also be used for high fidelity two-way quantum communication between the registers A and B . Indeed, the conditions (I) and (II) are adequate to construct a high-fidelity two-way quantum communication. For the case of $M=2$, consider the initial state $|\Psi_0\rangle=|\psi_1, \psi_2\rangle_A|\mathbf{0}\rangle_{ch}|\varphi_1, \varphi_2\rangle_B$ with $|\psi_1\rangle=|+\rangle$, $|\psi_2\rangle=|0\rangle$, $|\varphi_1\rangle=|0\rangle$, and $|\varphi_2\rangle=|1\rangle$, for instance. We aim to swap the initial states of registers A and B and,

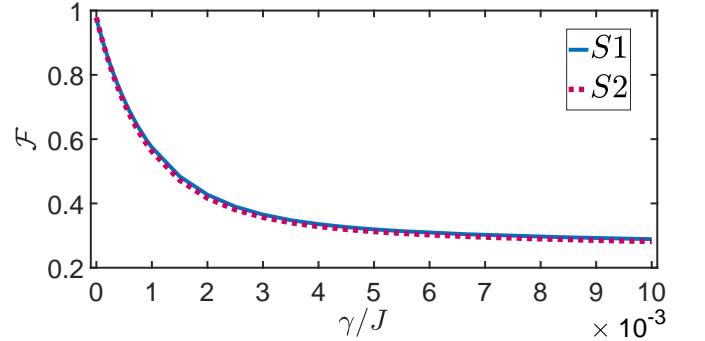


FIG. 4: Dephasing: The average $\mathcal{F}=(\bar{F}_1 + \bar{F}_2)/2$ for our two strategies $\mathcal{S}1$ and $\mathcal{S}2$ as a function of dephasing rate γ/J in a chain of $N=10$. The Hamiltonian parameters are taken as $\{J_0/J=0.04, h_1/J=0.45, h_2/J=-0.15\}$ and $\{h_0/J=26, h_1/J=0.2, h_2/J=-0.5\}$, respectively, for $\mathcal{S}1$ and $\mathcal{S}2$.

hence, obtain the final state as $|\Phi_T\rangle=|\varphi_1, \varphi_2\rangle_A|\mathbf{0}\rangle_{ch}|\psi_1, \psi_2\rangle_B$ up to a phase factor. Since by sitting in each qubit's site, e.g., A_1 , one can see that the information arrives from all other qubits, so $|\Phi_C\rangle=|\varphi_2, \varphi_1\rangle_A|\mathbf{0}\rangle_{ch}|\psi_2, \psi_1\rangle_B$ is a state that obtained because of the information flow between $\{A_1, B_1\}$ and $\{A_2, B_2\}$, causing the crosstalk. In Fig. 5(a) we plot $|\langle\Phi_T|e^{-iHt}|\Psi_0\rangle|^2$ and $|\langle\Phi_C|e^{-iHt}|\Psi_0\rangle|^2$ as the transmission fidelity and crosstalk, respectively, for our first strategy in a chain of $N=10$. The same quantity is plotted in Fig. 5(b) for the second strat-

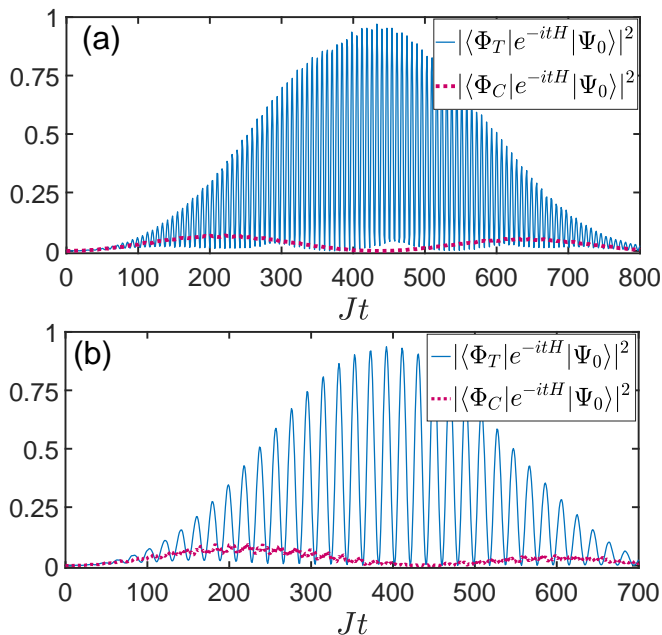


FIG. 5: Two-way communication: The transmission fidelity $|\langle \Phi_T | e^{-itH} | \Psi_0 \rangle|^2$ and the corresponding crosstalk $|\langle \Phi_C | e^{-itH} | \Psi_0 \rangle|^2$ for strategies **S1** (a) and **S2** (b) as a function of time in a chain of $N=10$. The Hamiltonian parameters are taken as $\{J_0^{opt}/J=0.04, h_1^{opt}/J=0.2, h_2^{opt}/J=-0.14\}$ and $\{h_0^{opt}/J=24, h_1^{opt}/J=0.45, h_2^{opt}/J=-0.5\}$, respectively, for **S1** and **S2**.

egy. In preparing these plots the Hamiltonian parameters are tuned appropriately to provide effective end-to-end interaction between each pair qubits. As the figures show, the transmission fidelities $|\langle \Phi_T | e^{-itH} | \Psi_0 \rangle|^2$ after some fluctuation reach to their highest values at a specific time while the crosstalk $|\langle \Phi_C | e^{-itH} | \Psi_0 \rangle|^2$ remains steadily negligible.

V. CONCLUSION

In order to be universal quantum computers, digital quantum simulators require the capability of performing

single- and two-qubit entangling gate operations. While the implementation of single-qubit gates relies on the capability of controlling individual particles and performing local unitary operations, the fulfillment of two-qubit entangling gates demands direct interaction between qubits which makes it more challenging, particularly, between distant qubits. One of the attractive approaches to mediate the interaction between remote qubits and realize a two-qubit entangling gate is to employ a spin chain data-bus and exploit the non-equilibrium dynamics of the system. In most of this type of gate implementation, only one gate can be performed at each time. This effectively restricts the computational power of the quantum processors through limiting the depth of the circuits. To overcome this limitation, here, we have devised a protocol that is able to implement multiple two-qubit entangling gates in parallel on arbitrary pairs of distant qubits through a commonly shared spin chain data-bus. Remarkably, while our protocol implements entangling gate between several pairs of qubits simultaneously, it keeps the crosstalk negligible through making each pair of qubits off-resonant from the others by local tuning of the magnetic fields. We have put forward two different strategies to achieve these goals through optimizing different sets of Hamiltonian parameters. Each of these strategies might be more convenient for certain physical platforms. Surprisingly, our protocol is hardly affected by increasing the length of the data-bus and the number of users. In addition, we showed that our protocol can realize two-way communication and tolerant decoherence effects.

VI. ACKNOWLEDGEMENT

AB acknowledges support from the National Key R&D Program of China, Grant No.2018YFA0306703.

-
- [1] A. Barenco, C. H. Bennett, R. Cleve, D. P. DiVincenzo, N. Margolus, P. Shor, T. Sleator, J. A. Smolin, and H. Weinfurter, *Phys. Rev. A* **52**, 3457 (1995).
 - [2] M. J. Bremner, C. M. Dawson, J. L. Dodd, A. Gilchrist, A. W. Harrow, D. Mortimer, M. A. Nielsen, and T. J. Osborne, *Phys. Rev. Lett.* **89**, 247902 (2002).
 - [3] M. D. Shulman, O. E. Dial, S. P. Harvey, H. Bluhm, V. Umansky, and A. Yacoby, *Science* **336**, 202 (2012).
 - [4] M. Veldhorst, C. H. Yang, J. C. Hwang, W. Huang, J. P. Dehollain, J. T. Muhonen, S. Simmons, A. Laucht, F. E. Hudson, K. M. Itoh, et al., *Nature* **526**, 410 (2015).
 - [5] Y. He, S. K. Gorman, D. Keith, L. Kranz, J. G. Keizer, and M. Y. Simmons, *Nature* **571**, 371 (2019).
 - [6] O. Mandel, M. Greiner, A. Widera, T. Rom, T. W. Hänsch, and I. Bloch, *Nature* **425**, 937 (2003).
 - [7] I. Bloch, *Nature* **453**, 1016 (2008).
 - [8] V. M. Schäfer, C. J. Ballance, K. Thirumalai, L. J. Stephenson, T. G. Ballance, A. M. Steane, and D. M. Lucas, *Nature* **555**, 75 (2018).
 - [9] C. J. Ballance, T. P. Harty, N. M. Linke, M. A. Sepiol, and D. M. Lucas, *Phys. Rev. Lett.* **117**, 060504 (2016).
 - [10] T. P. Harty, D. T. C. Allcock, C. J. Ballance, L. Guidoni, H. A. Janacek, N. M. Linke, D. N. Stacey, and D. M. Lucas, *Phys. Rev. Lett.* **113**, 220501 (2014).
 - [11] C. J. Ballance, T. P. Harty, N. M. Linke, M. A. Sepiol, and D. M. Lucas, *Phys. Rev. Lett.* **117**, 060504 (2016).
 - [12] J. P. Gaebler, T. R. Tan, Y. Lin, Y. Wan, R. Bowler, A. C. Keith, S. Glancy, K. Coakley, E. Knill, D. Leibfried, et al., *Phys. Rev. Lett.* **117**, 060505 (2016).
 - [13] R. Barends, J. Kelly, A. Megrant, A. Veitia, D. Sank, E. Jeffrey,

- T. C. White, J. Mutus, A. G. Fowler, B. Campbell, et al., *Nature* **508**, 500 (2014).
- [14] B. Foxen, C. Neill, A. Dunsworth, P. Roushan, B. Chiaro, A. Megrant, J. Kelly, Z. Chen, K. Satzinger, R. Barends, et al., arXiv:2001.08343 (2020).
- [15] D. Yu, H. Wang, D. Ma, X. Zhao, and J. Qian, *Opt. Express* **27**, 23080 (2019).
- [16] Y.-Y. Huang, Y.-K. Wu, F. Wang, P.-Y. Hou, W.-B. Wang, W.-G. Zhang, W.-Q. Lian, Y.-Q. Liu, H.-Y. Wang, H.-Y. Zhang, et al., *Phys. Rev. Lett.* **122**, 010503 (2019).
- [17] B. Bertrand, S. Hermelin, S. Takada, M. Yamamoto, S. Tarucha, A. Ludwig, A. D. Wieck, C. Bäuerle, and T. Meunier, *Nature Nanotech.* **11**, 672 (2016).
- [18] T. Fujita, T. A. Baart, C. Reichl, W. Wegscheider, and L. M. K. Vandersypen, *npj Quantum Inf.* **3**, 22 (2017).
- [19] A. R. Mills, D. M. Zajac, M. J. Gullans, F. J. Schupp, T. M. Hazard, and J. R. Petta, *Nat. Commun.* **10**, 1 (2019).
- [20] A. Bienfait, K. J. Satzinger, Y. P. Zhong, H. S. Chang, M. H. Chou, C. R. Conner, Dumur, J. Grebel, G. A. Peairs, R. G. Povey, et al., *Science* **364**, 368 (2019).
- [21] D. L. Moehring, P. Maunz, S. Olmschenk, K. C. Younge, D. N. Matsukevich, L.-M. Duan, and C. Monroe, *Nature* **449**, 68 (2007).
- [22] E. Togan, Y. Chu, A. S. Trifonov, L. Jiang, J. Maze, L. Childress, M. G. Dutt, A. S. Sørensen, P. Hemmer, A. S. Zibrov, et al., *Nature* **466**, 730 (2010).
- [23] P. Campagne-Ibarcq, E. Zalys-Geller, A. Narla, S. Shankar, P. Reinhold, L. Burkhardt, C. Axline, W. Pfaff, L. Frunzio, R. J. Schoelkopf, et al., *Phys. Rev. Lett.* **120**, 200501 (2018).
- [24] J. I. Cirac and P. Zoller, *Phys. Rev. Lett.* **74**, 4091 (1995).
- [25] P. Rabl, S. J. Kolkowitz, F. Koppens, J. Harris, P. Zoller, and M. D. Lukin, *Nature Phys.* **6**, 602 (2010).
- [26] S. Bose, *Phys. Rev. Lett.* **91**, 207901 (2003).
- [27] A. Bayat and S. Bose, *Phys. Rev. A* **81**, 012304 (2010).
- [28] S. Yang, A. Bayat, and S. Bose, *Phys. Rev. A* **84**, 020302 (2011).
- [29] N. Y. Yao, L. Jiang, A. V. Gorshkov, Z.-X. Gong, A. Zhai, L.-M. Duan, and M. D. Lukin, *Phys. Rev. Lett.* **106**, 040505 (2011).
- [30] S. J. Blundell and F. L. Pratt, *J. Phys.: Condens. Matter* **16**, R771 (2004).
- [31] F. A. Zwanenburg, A. S. Dzurak, A. Morello, M. Y. Simmons, L. C. Hollenberg, G. Klimeck, S. Rogge, S. N. Coppersmith, and M. A. Eriksson, *Rev. Mod. Phys.* **85**, 961 (2013).
- [32] R. Fazio and H. Van Der Zant, *Phys. Rep.* **355**, 235 (2001).
- [33] D. Porras and J. I. Cirac, *Phys. Rev. Lett.* **92**, 207901 (2004).
- [34] R. Blatt and C. F. Roos, *Nature Phys.* **8**, 277 (2012).
- [35] L. Banchi, A. Bayat, P. Verrucchi, and S. Bose, *Phys. Rev. Lett.* **106**, 140501 (2011).
- [36] M.-H. Yung and S. Bose, *Phys. Rev. A* **71**, 032310 (2005).
- [37] M.-H. Yung, S. C. Benjamin, and S. Bose, *Phys. Rev. Lett.* **96**, 220501 (2006).
- [38] A. V. Gorshkov, J. Otterbach, E. Demler, M. Fleischhauer, and M. D. Lukin, *Phys. Rev. Lett.* **105**, 060502 (2010).
- [39] H. Weimer, N. Y. Yao, C. R. Laumann, and M. D. Lukin, *Phys. Rev. Lett.* **108**, 100501 (2012).
- [40] T. J. G. Apollaro, S. Lorenzo, A. Sindona, S. Paganelli, G. Giorgi, and F. Plastina, *Phys. Scr.* **2015**, 014036 (2015).
- [41] W. J. Chetcuti, C. Sanavio, S. Lorenzo, and T. J. G. Apollaro, *New J. Phys.* **22**, 033030 (2020).
- [42] D. Aharonov and M. Ben-Or, *SIAM J. Comput.* **38**, 1207 (2008).
- [43] A. M. Steane, *Fortschr. Phys.* **46**, 443 (1998).
- [44] C. Figgatt, A. Ostrander, N. M. Linke, K. A. Landsman, D. Zhu, D. Maslov, and C. Monroe, *Nature* **572**, 368 (2019).
- [45] N. Grzesiak, R. Blümel, K. Wright, K. M. Beck, N. C. Pisenti, M. Li, V. Chaplin, J. M. Amini, S. Debnath, J. S. Chen, et al., *Nature Commun.* **11**, 1 (2020).
- [46] Z.-M. Wang, C. A. Bishop, Y.-J. Gu, and B. Shao, *Phys. Rev. A* **84**, 022345 (2011).
- [47] R. Yousefjani and A. Bayat, *Phys. Rev. A* **102**, 012418 (2020).
- [48] A. Bayat and Y. Omar, *New J. Phys.* **17**, 103041 (2015).
- [49] T. J. G. Apollaro, C. Sanavio, W. J. Chetcuti, and S. Lorenzo, *Phys. Lett. A* **384**, 126306 (2020).
- [50] A. Wójcik, T. Łuczak, P. Kurzyński, A. Grudka, T. Gdala, and M. Bednarska, *Phys. Rev. A* **72**, 034303 (2005).
- [51] L. C. Venuti, C. D. E. Boschi, and M. Roncaglia, *Phys. Rev. Lett.* **96**, 247206 (2006).
- [52] L. C. Venuti, S. Giampaolo, F. Illuminati, and P. Zanardi, *Phys. Rev. A* **76**, 052328 (2007).
- [53] S. Paganelli, S. Lorenzo, T. J. G. Apollaro, F. Plastina, and G. L. Giorgi, *Phys. Rev. A* **87**, 062309 (2013).
- [54] S. Lorenzo, T. J. G. Apollaro, A. Sindona, and F. Plastina, *Phys. Rev. A* **87**, 042313 (2013).
- [55] R. Lewis-Swan, A. Safavi-Naini, A. Kaufman, and A. Rey, *Nat. Rev. Phys.* **1**, 627 (2019).
- [56] J. Eisert, M. Friesdorf, and C. Gogolin, *Nature Phys.* **11**, 124 (2015).
- [57] M. A. Nielsen, *Phys. Lett. A* **303**, 249 (2002).